Reversible CO_2 induced gate-opening and closing pressures in 2D rare earth-oxalate coordination networks

Issaraporn Rakngam,[a] Kulwadee Ponanunrirk,[a] Kenika Khotchasanthong,[a]
Pacharapon Jearanaiwiwat,[a] Chombongkot Sricharoen,[a] Phasini Kasantikul,[b] Satida Prasantree,[b]
Bunyarat Rungtaweevoranit,[c] Sakchai Laksee,[d] and Kittipong Chainok*[a,e]

[a] Thammasat University Research Unit in Multifunctional Crystalline Materials and Applications (TU-McMa), Faculty of Science and Technology, Thammasat University, Pathum Thani 12121, Thailand. E-mail: kc@tu.ac.th; Fax: +662 654 4548; Tel: +66 86 339 5079

[b] Science Classrooms in University-Affiliated School Project Thammasat University-Suankulabwittayalai Rangsit (SCiUS TU-SKR), Pathum Thani 12121, Thailand

[c] National Nanotechnology Center (NANOTEC), National Science and Technology Development Agency (NSTDA), Pathum Thani 12120, Thailand

[d] Thailand Institute of Nuclear Technology (Public Organization), Nakhon Nayok 26120, Thailand

[e] Center of Excellence on Petrochemical and Materials Technology, Chulalongkorn University, Bangkok 10330, Thailand

Table S1 Selected bond lengths (Å) and bond angles (°) for all compounds in the series **1RE**.

	1Ce	**1Pr**	**1Nd**	**1Sm**
RE1–O1	2.520 (2)	2.506 (3)	2.487 (6)	2.465 (4)
RE1–O2^{i}	2.490 (2)	2.471 (3)	2.460 (6)	2.430 (4)
RE1–O3	2.535 (2)	2.519 (4)	2.495 (6)	2.459 (4)
RE1–O4^{i}	2.579 (2)	2.560 (3)	2.541 (6)	2.511 (4)
RE1–O5	2.532 (2)	2.517 (4)	2.496 (6)	2.471 (4)
RE1–O6^{ii}	2.497 (2)	2.479 (3)	2.463 (6)	2.430 (4)
RE1–O7	2.526 (2)	2.506 (3)	2.498 (6)	2.456 (4)
RE1–O8^{ii}	2.541 (2)	2.525 (4)	2.509 (6)	2.481 (4)
RE1–O9	2.638 (2)	2.623 (3)	2.612 (6)	2.609 (3)
O1–RE1–O3	63.99 (7)	64.47 (11)	64.94 (19)	111.94 (13)
O1–RE1–O4^{i}	112.89 (7)	112.66 (12)	112.6 (2)	71.74 (13)
O1–RE1–O5	72.60 (7)	72.47 (12)	71.9 (2)	71.36 (13)
O1–RE1–O7	78.08 (8)	77.86 (13)	77.9 (2)	122.1 (2)
O1–RE1–O8^{ii}	72.17 (7)	72.00 (12)	71.8 (2)	144.46 (16)
O1–RE1–O9	120.43 (9)	120.85 (15)	121.8 (3)	138.57 (12)
O2^{i}–RE1–O1	145.17 (8)	145.13 (13)	144.7 (2)	65.76 (13)
O2^{i}–RE1–O3	140.75 (7)	139.95 (12)	139.6 (2)	75.00 (16)
O2^{i}–RE1–O4^{i}	64.08 (7)	64.63 (11)	64.7 (2)	77.88 (15)
O2^{i}–RE1–O5	74.53 (8)	74.73 (13)	75.0 (2)	130.85 (13)
O2^{i}–RE1–O6^{ii}	86.22 (7)	85.72 (12)	85.8 (2)	70.9 (4)
O2^{i}–RE1–O7	77.53 (8)	77.69 (13)	77.5 (2)	65.56 (13)
O2^{i}–RE1–O8^{ii}	128.59 (7)	129.12 (12)	129.6 (2)	143.34 (15)
O2^{i}–RE1–O9	72.74 (14)	72.2 (3)	70.9 (6)	134.11 (13)
O3–RE1–O4^{i}	142.80 (7)	142.89 (12)	143.3 (2)	76.29 (15)
O3–RE1–O8^{ii}	76.13 (8)	76.30 (13)	134.0 (2)	67.7 (4)
O3–RE1–O9	68.11 (13)	67.8 (3)	90.2 (2)	126.0 (2)
O4^{i}–RE1–O9	126.67 (9)	126.47 (15)	76.4 (2)	68.86 (14)
O5–RE1–O3	133.80 (7)	134.07 (11)	68.8 (6)	105.59 (12)
O5–RE1–O4^{i}	68.84 (7)	68.81 (12)	125.6 (3)	127.9 (4)
O5–RE1–O8^{ii}	105.54 (7)	105.48 (11)	68.8 (2)	129.77 (16)
O5–RE1–O9	127.64 (14)	127.9 (3)	65.0 (2)	85.28 (14)
O6^{ii}–RE1–O1	127.99 (7)	128.58 (12)	105.2 (2)	79.26 (14)
O6^{ii}–RE1–O3	78.59 (7)	78.86 (12)	127.0 (5)	76.33 (14)
O6^{ii}–RE1–O4^{i}	76.49 (8)	76.27 (12)	128.9 (2)	144.61 (15)
O6^{ii}–RE1–O5	144.98 (8)	144.64 (12)	78.8 (2)	138.62 (12)
O6^{ii}–RE1–O7	140.12 (7)	139.69 (11)	76.5 (2)	66.11 (13)
O6^{ii}–RE1–O8^{ii}	64.43 (7)	64.93 (11)	144.9 (2)	69.3 (3)
O6^{ii}–RE1–O9	70.76 (10)	70.3 (2)	139.1 (2)	77.31 (14)
O7–RE1–O3	91.36 (7)	90.64 (12)	65.3 (2)	88.85 (14)
O7–RE1–O4^{i}	125.22 (7)	125.89 (12)	70.5 (3)	127.28 (15)
O7–RE1–O5	64.08 (7)	64.61 (11)	126.0 (2)	65.61 (13)
O7–RE1–O8^{ii}	150.25 (7)	149.86 (12)	149.7 (2)	148.58 (14)
O7–RE1–O9	69.69 (11)	69.7 (2)	68.8 (4)	69.5 (3)
O8^{ii}–RE1–O4^{i}	68.35 (7)	68.38 (11)	68.8 (2)	68.98 (13)
O8^{ii}–RE1–O9	126.82 (14)	126.7 (3)	127.8 (5)	126.5 (4)

Symmetry codes: (i) −*x*+3/2, *y*−1/2, *z*+1/2; (ii) −*x*+3/2, *y*−1/2, *z*−1/2; (iii) −*x*+3/2, *y*+1/2, *z*−1/2; (iv) −*x*+3/2, *y*+1/2, *z*+1/2.

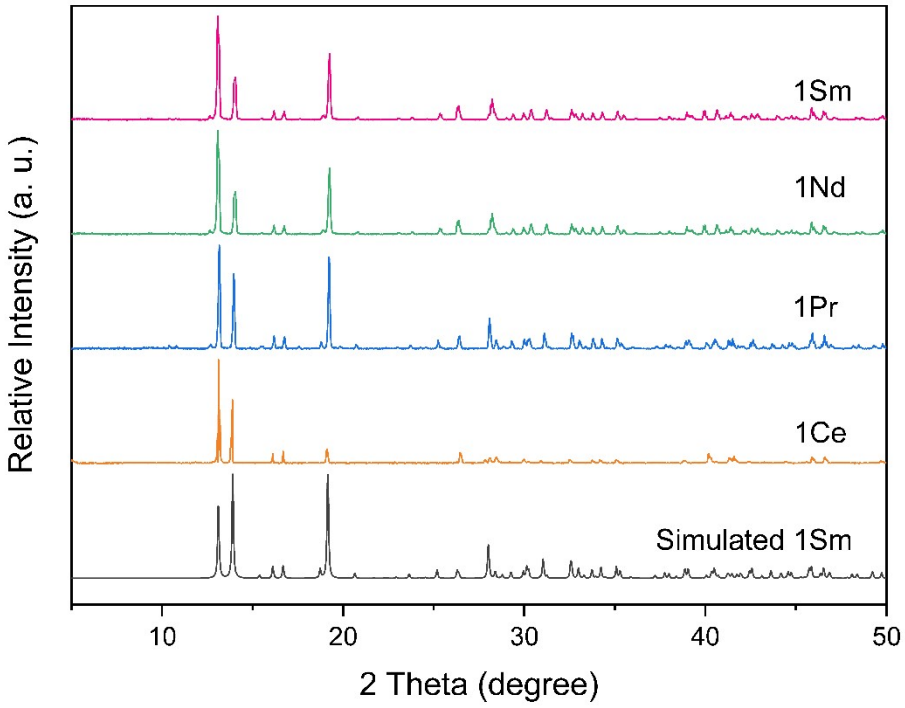

Fig. S1 Comparison of the simulated and as-synthesized PXRD patterns of all compounds in the series **1RE**.

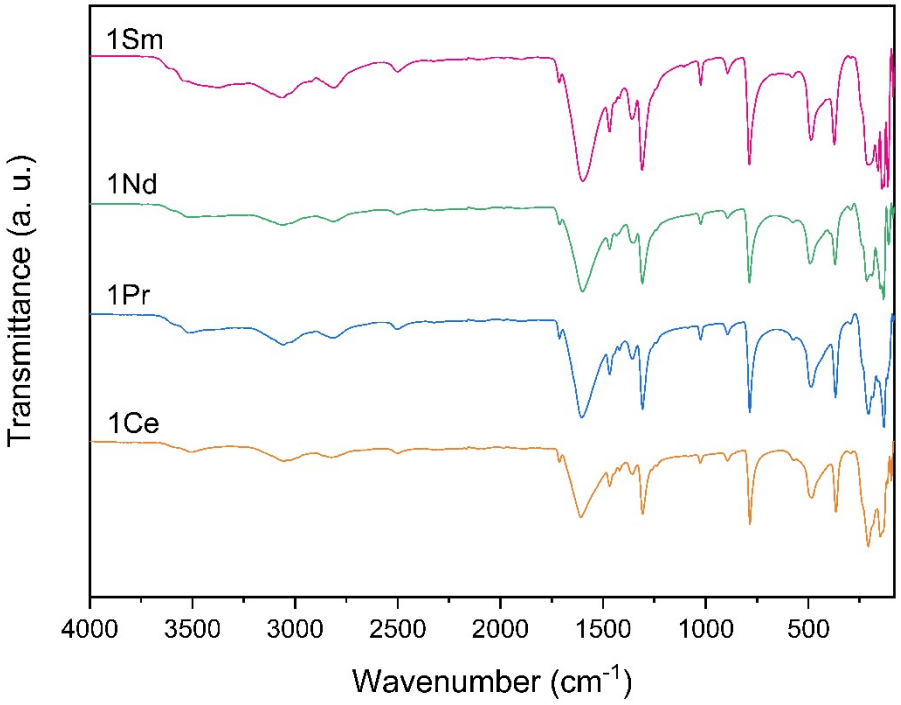

Fig. S2 FTIR spectra of all compounds in the series **1RE**.

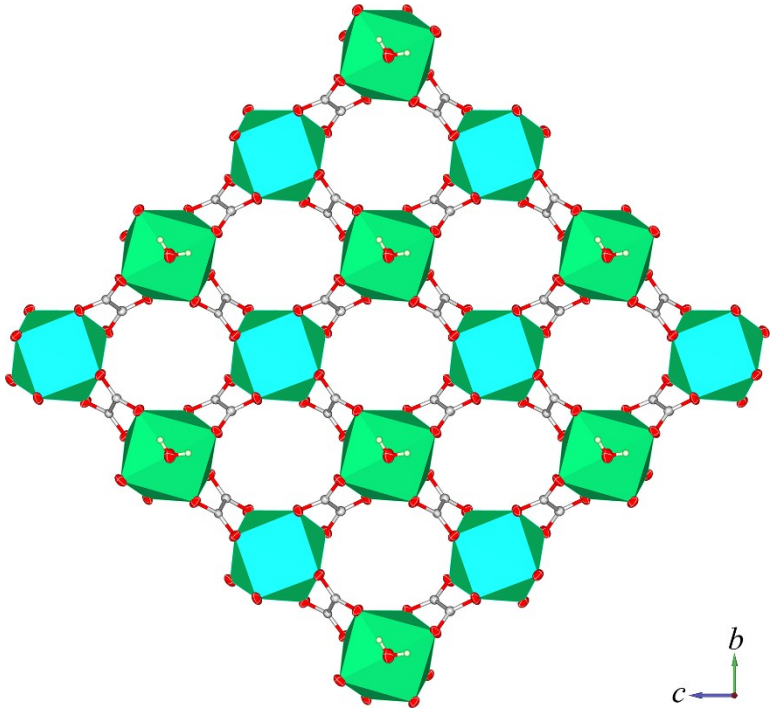

Fig. S3 A single layer [Sm(ox)(H_2O)] structure extended in the *bc* plane.

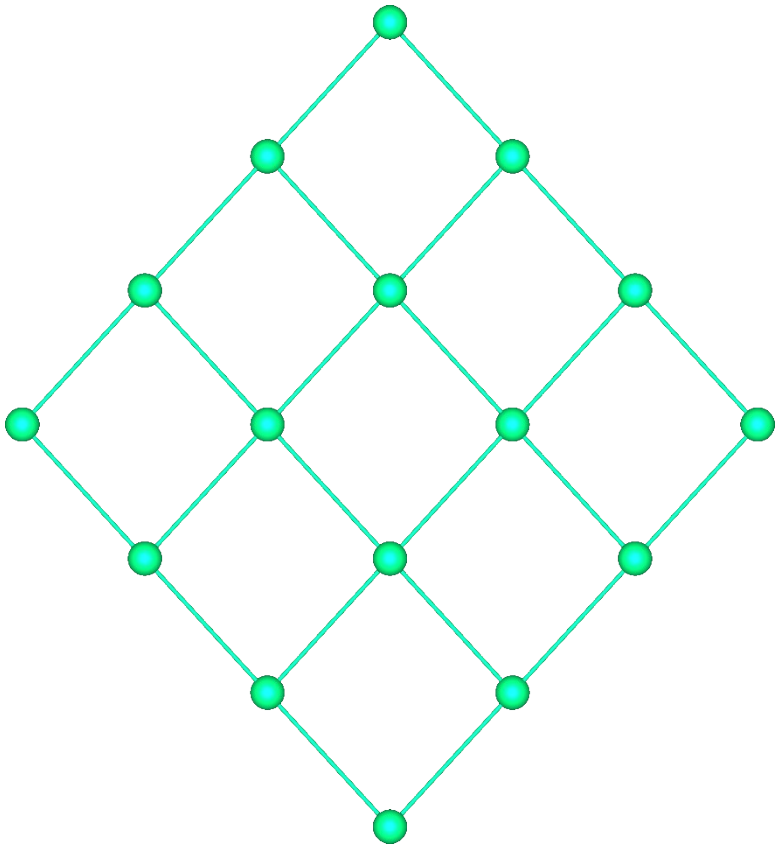

Fig. S4 Depiction of the square lattice (*sql*) topology type of **1Sm**.

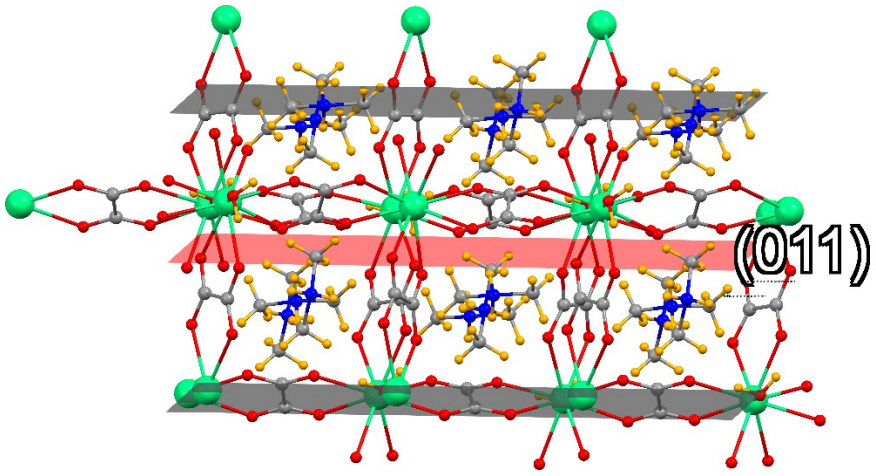

(a)

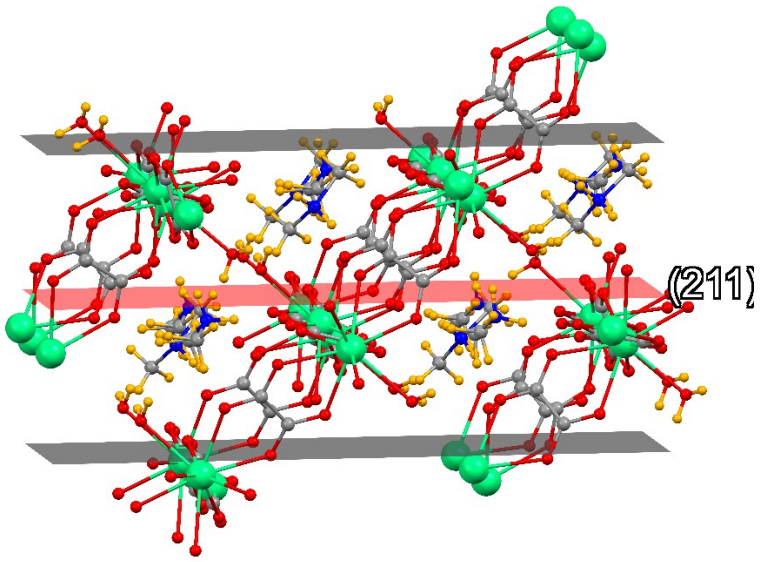

(b)

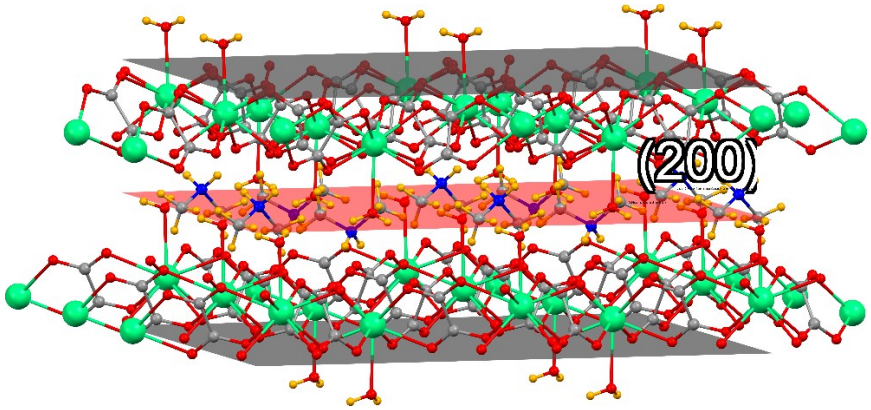

(c)

Fig. S5 Illustration of slice (a) (011), (b) (211), and (c) (200) planes created with Mercury v. 2024.3.1 software.

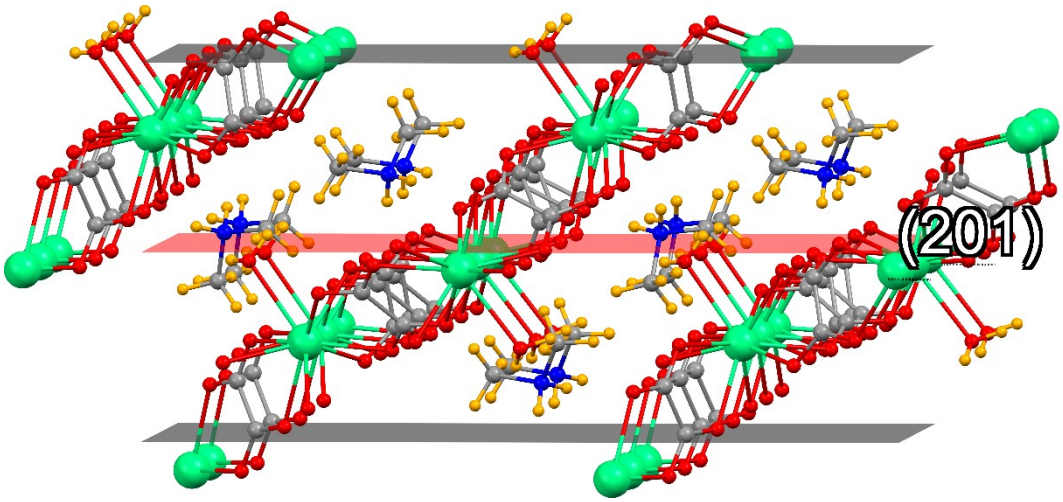

(a)

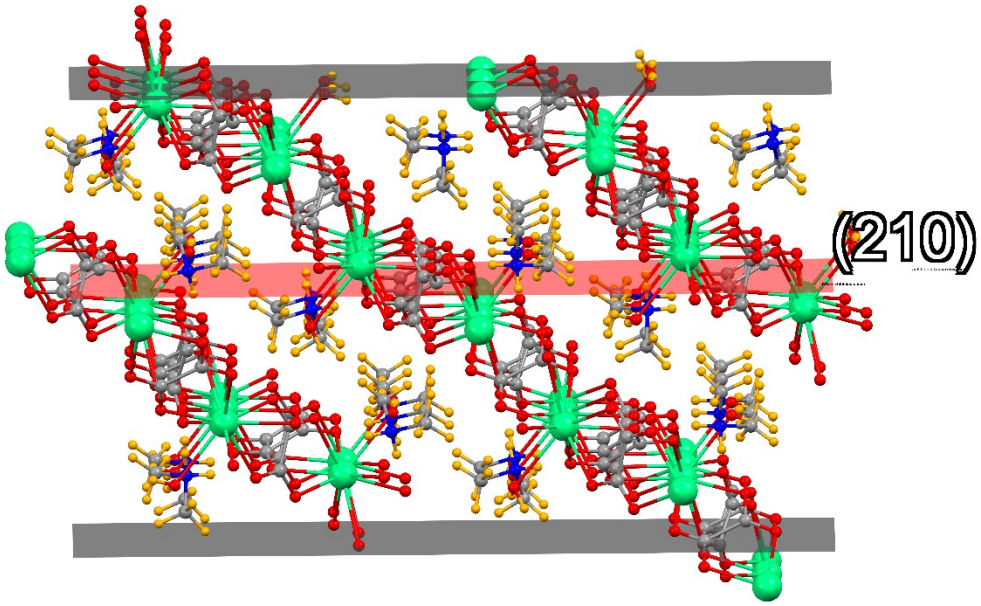

(b)

Fig. S6 Depiction of slice (a) (201) and (b) (210) planes created with Mercury v. 2024.3.1 software.

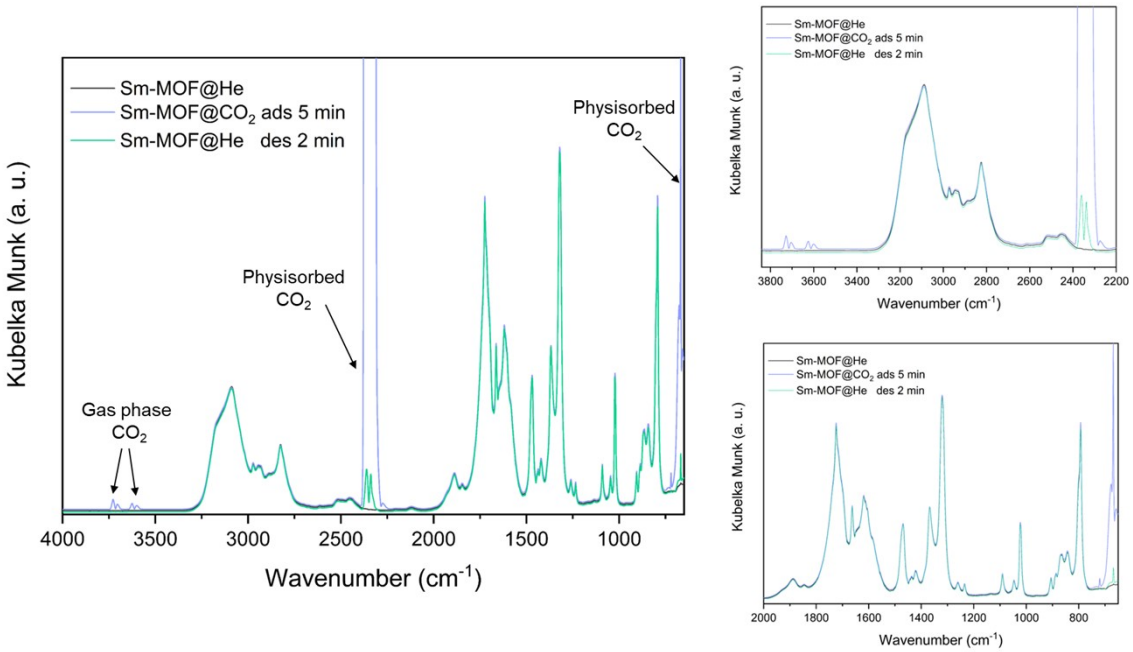

Fig. S7. In situ DRIFT spectra of **1Sm** at 273 K and 1 bar during CO_2 adsorption and desorption.

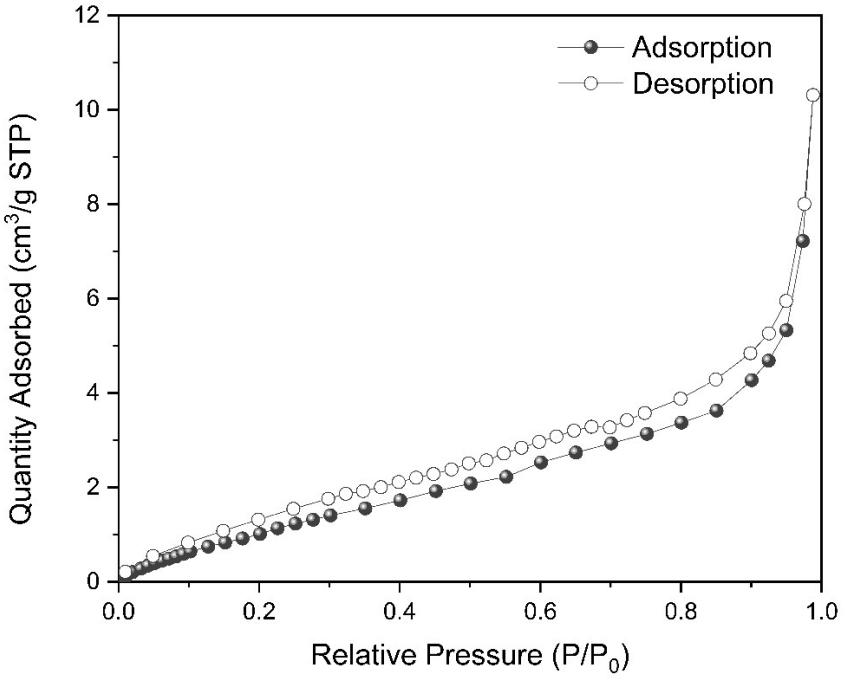

Fig. S8 N_2 sorption isotherm for **1Sm** at 77K.

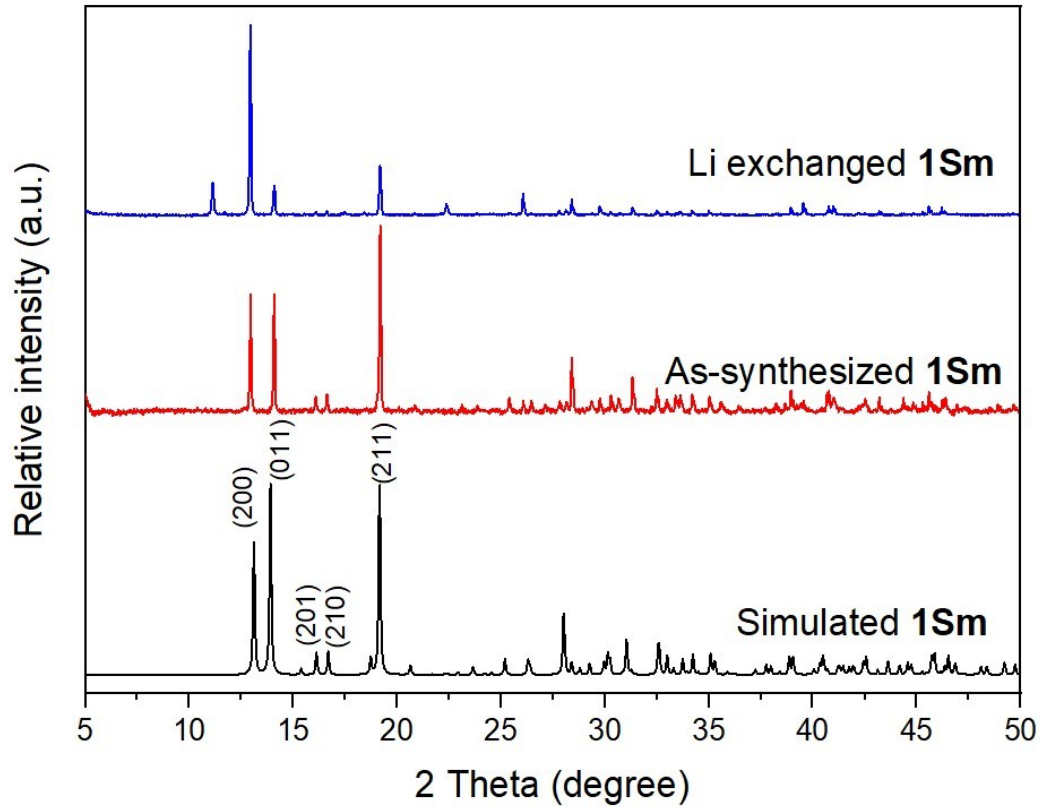

Fig. S9 Comparison of PXRD patterns for simulated, as-synthesized, and lithium(I) exchanged **1Sm**.

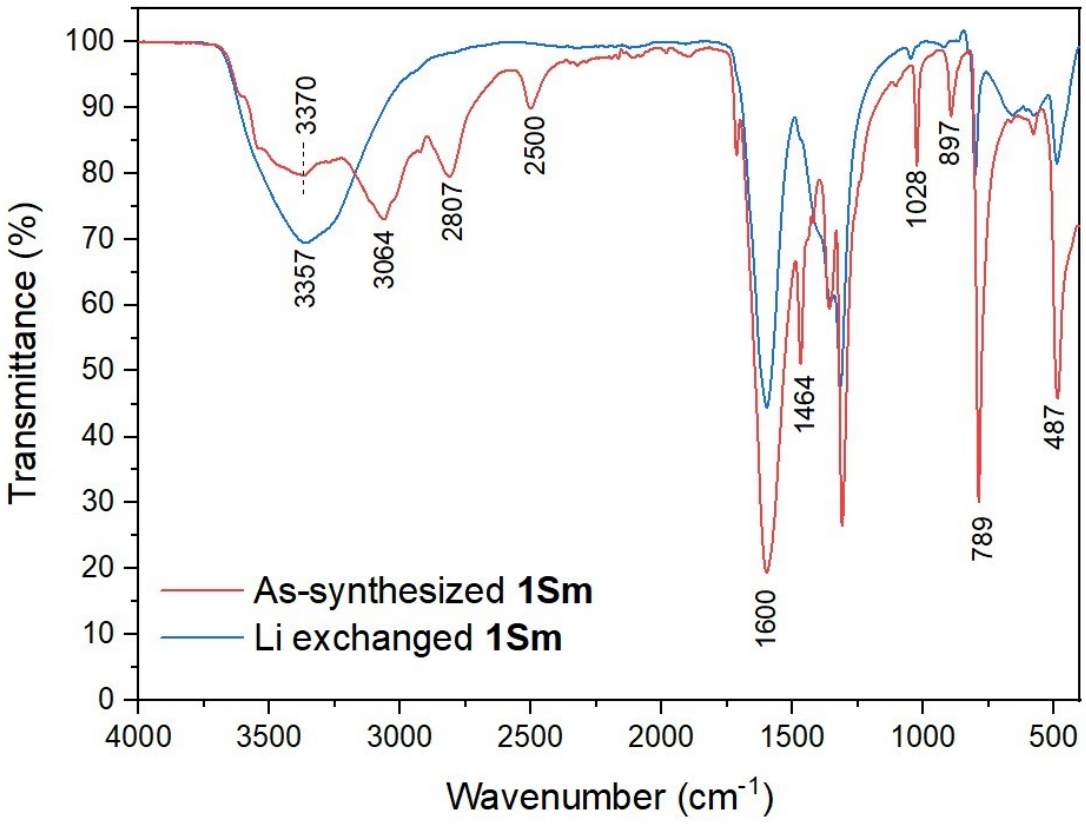

Fig. S10 Comparison IR spectra for as-synthesized and lithium(I) exchanged **1Sm**.

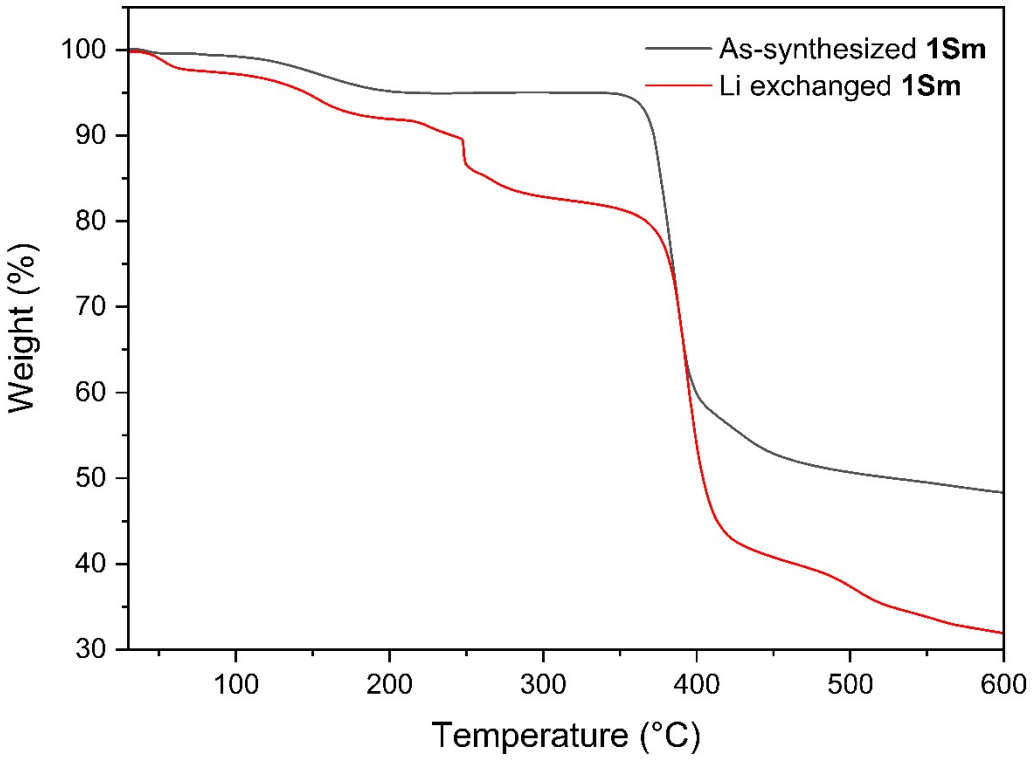

Fig. S11 Comparison TGA curves for as-synthesized and lithium(I) exchanged **1Sm**.

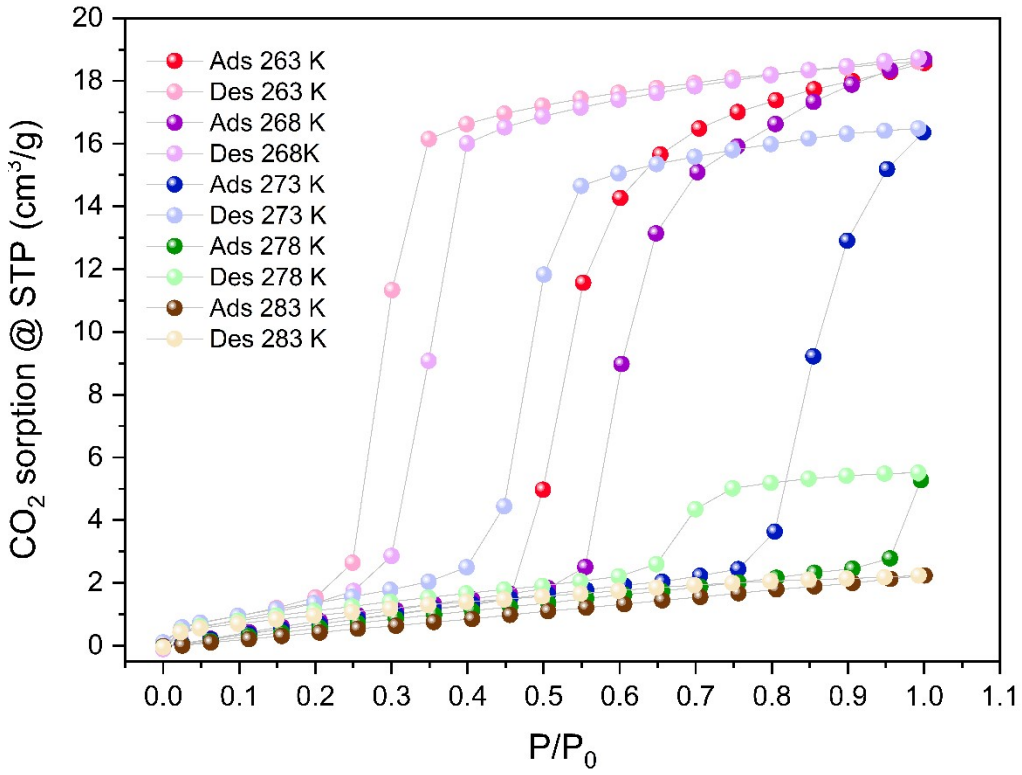

Fig. S12 Temperature-dependent CO_2 adsorption-desorption isotherms for lithium(I)-exchanged **1Sm** up to 1 bar at temperatures between 263 and 283 K.